

Article

Fatigue Property and Improvement of a Rounded Welding Region between the Diaphragm Plate and Closed Rib of an Orthotropic Steel Bridge Deck

Datao Li * , Chunguo Zhang and Pengmin Lu *

Key Laboratory of Road Construction Technology and Equipment, MOE, Chang'an University, Xi'an 710064, China; zcguo2008@163.com

* Correspondence: ldt1688@chd.edu.cn (D.L.); lpmin@chd.edu.cn (P.L.)

Received: 31 December 2019; Accepted: 20 January 2020; Published: 21 January 2020



Abstract: By means of finite element modeling (FEM) and fatigue experiments, we study the fatigue performance of the rounded welding region between the diaphragm plate and closed rib of orthotropic steel bridge deck in this work. A local sub-model of the rounded welding region from the orthotropic steel bridge deck was developed to analyze the stress distributions. Based on the analysis results we designed the fatigue specimen for the fatigue test of this detailed structure. The fatigue experimental results revealed that the crack initiates from the weld toe of the rounded welding region and the stress concentration at the rounded welding region is the main mechanism of fatigue crack initiation. In addition, we propose three improvements to reduce the stress concentration of the rounded welding region, and the local structure optimization scheme of the diaphragm–rib weld can effectively improve the fatigue resistance of the detailed weld structure.

Keywords: fatigue performance; rounded welding region; finite element modeling (FEM); structure optimization; reinforcing plate

1. Introduction

The orthotropic steel bridge decks are used in most of the world's major long span bridges with an important character of low dead weight. The orthotropic steel deck consists of a deck plate supported in mutually perpendicular directions; all these elements are connected by welded connections. Owing to the cyclic load stress caused by a high number of vehicles, fatigue cracks in orthotropic steel bridges significantly occur at partial-penetration fillet-welded connections [1–7]. Usually, enhancing the fatigue strength of welded joints, such as the rib-to-rib welded details, rib-to-crossbeam welded joints, and field splice joints of longitudinal ribs [3,8–10] is an effective method to improve the fatigue resistance of the orthotropic steel decks.

Till now, numerous works have focused on the fatigue behaviors of structure details in orthotropic bridges decks. Taking orthotropic decks of the Williamsburg Bridge for instance, Tsakopoulos and Fisher [11] studied fatigue resistance of local welding structure between rib and diaphragm, and the observations are recommended in the 1994 AASHTO LRFD Bridge Design Specifications. Several modifications are proposed for orthotropic deck design and some modifications are adopted in the 2000 Interim AASHTO LRFD Specifications. In addition, Connor and Fisher [12] explored an identical method to examine how fatigue stress range is defined and determined during the testing, then the fatigue resistance of welded rib-to-web connections in steel orthotropic bridge decks is obtained. Furthermore, Xiao et al. [13] evaluated the stress distributions and fatigue life of the rib-deck welded joints in orthotropic steel decks using finite element modeling (FEM). Ya et al. [14] further measured the fatigue behavior of rib-deck welded joints on the orthotropic steel bridge deck. Moreover, the

effects of fabrication procedures on fatigue resistance of welded joints in orthotropic steel decks have also been discussed [15]. Miki [16] used the FE sub-models of rib-to-deck joint derived from the global model of a real bridge to investigate the notch stresses at the weld root, the observations show the increase of the weld penetration results in the higher fatigue resistance. In addition, the effects of concrete cracking on the stress range response of welded joint in rib-to-floor beam can be evaluated through the FE analysis [17].

Although numerous efforts have been invested into the weld fatigue of the orthotropic steel bridge deck, the investigations on fatigue behaviors of the rounded welding region between diaphragm plate and closed rib are still under-researched. Facing to the fatigue behavior of this structure detail, we may think about a question, i.e., how does the fatigue behavior of this detail perform under cyclic loading? In this study, we attempt to answer this question using experimental method and FEM. In addition, this study is organized as follows: Firstly, we design fatigue specimens based on the simulated stress distributions of the detailed structures. Then, we perform the fatigue tests of specimens (nine specimens) and obtain the fatigue strength. Finally, we propose three schemes to improve the fatigue strength of this detail, and find that scheme 2 can effectively reduce the stress concentration of the rounded welding region.

2. Experiment

2.1. Design of Fatigue Specimen

According to the general code for design of highway bridges and culverts [18], we could analyze the stress distribution of the detailed structure in the orthotropic steel bridge deck. Firstly, the standard load of a vehicle for the stress analysis is chosen as 550 kN, the axle-loads for the middle and rear are 2×120 kN and 2×140 kN, respectively. In addition, the wheel contact area of two tires is assumed as a rectangle of 600 mm \times 200 mm. The thickness of the asphalt pavement layer is about 55 mm and the load distribution angle is 45°. Thus, the actual load area on the deck is 710 mm \times 310 mm, as shown in Figure 1. Moreover, we choose a bridge deck (3750 mm \times 4800 mm) as the stress analysis object (Figure 2). Based on the aforementioned standard, an assumed truck wheel load along the transverse direction of the bridge deck is used to determine the maximum stress of our interest point (Figure 2). Furthermore, an FE model consisting of a diaphragm and eight closed ribs is created in ANSYS software. In this model, Shell63 element is applied in the FE model, and it contains about 83800 elements and 83500 nodes. For the FE model, the bottom of the diaphragm is fully fixed. At one side of the closed rib, the freedoms in the Y and Z directions are restrained. For the other end, the freedom in the Y direction is fixed. The location of the rear axle (2×140 kN) is just on the top of the diaphragm (Figure 1). In addition, for the FE model, we can find a similar mesh generation in Ref. [13]. Moreover, in Figure 1, we can see the rounded welding region of the orthotropic steel bridge deck as shown in the red-squared part in the A direction. Usually, the fatigue crack initiates in the weld toe of the rounded welding region.

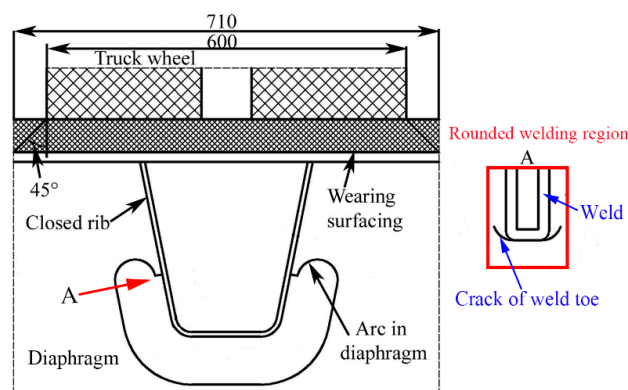


Figure 1. Fatigue crack of the rounded welding region between a closed rib and a diaphragm (in mm).

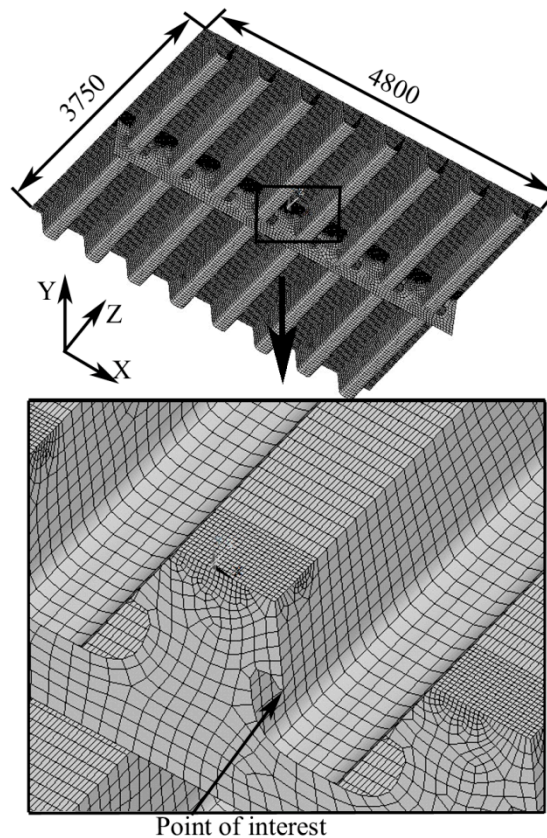


Figure 2. finite element (FE) model and the interest point of the rounded welding region.

Moreover, Figure 3a exhibits a simulated maximum principal stress–time curve of the interest point when the wheel loads are running along the transverse direction (Z direction in Figure 2) of the bridge deck. And the wheels load just locates on the diaphragm and closed rib when the maximum principal stress reaches the maximum value as shown in the curve (Figure 3b). Furthermore, a sub-model is developed to simulate the stress distribution around the interest point. Then, the boundary conditions applied to the sub-model are obtained from the FE model as shown in Figure 3b as the maximum principal stress reaches the maximum value (Figure 3a). In the sub-model, the element (Solid185, it is a 3-dimensional solid element with eight nodes in ANSYS software) sizes of the weld are about 2~3 mm (Figure 4). In addition, a schematic diagram of the diaphragm–rib structure of an orthotropic steel bridge deck and the weld details of interest regions are shown in Figure 5.

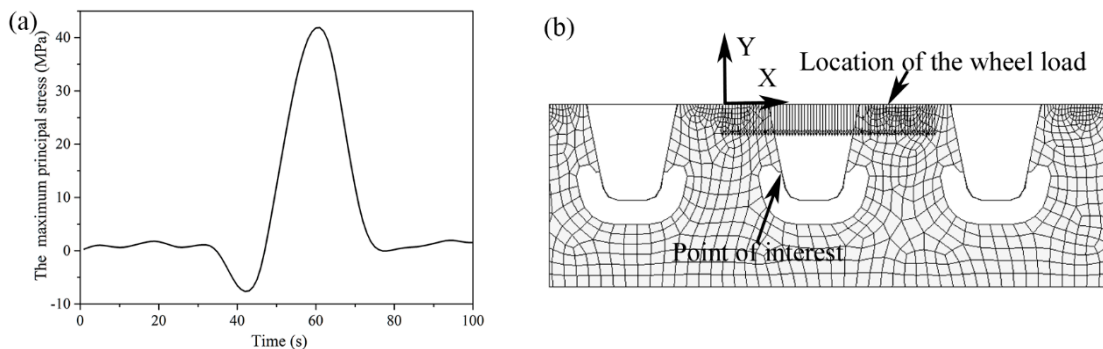


Figure 3. (a) Maximum principal stress–time curve of the interest point, and (b) the position of wheel load as the maximum principal stress of the interest point reaches its peak.

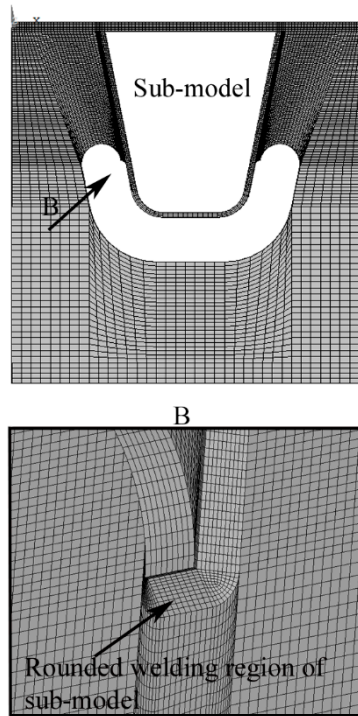


Figure 4. Sub-model of the rounded welding region.

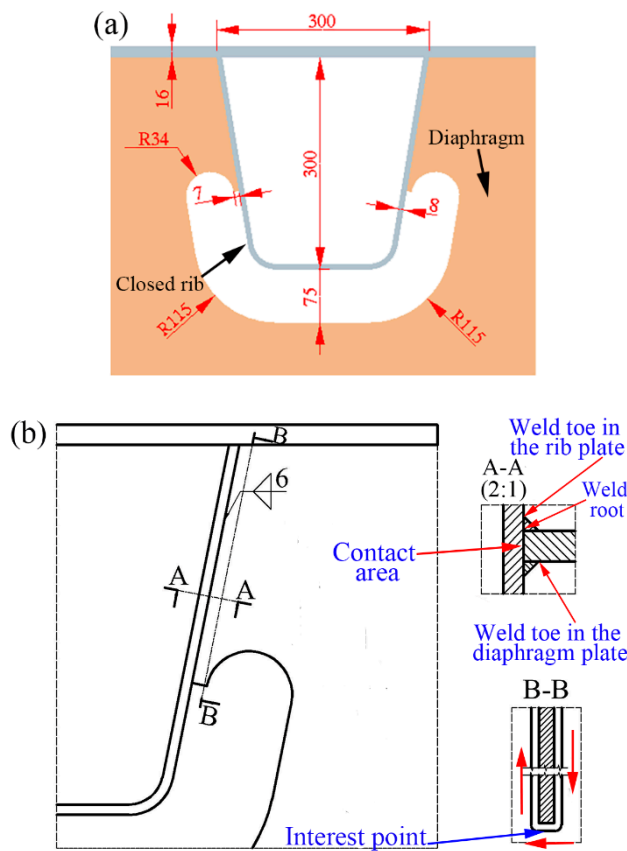


Figure 5. (a) Structure schematic diagram (in mm) and (b) the fillet weld between closed rib and diaphragm (in mm).

As shown in Figure 5b, double-sided fillet welds are adopted for welding the diaphragm and the closed rib, and the weld width is about 6 mm. The contact elements are created on the contact area

between the diaphragm and the closed rib. In addition, the cross section of the fillet weld is a triangular shape (partial view A-A in Figure 5b), the weld toes (in the diaphragm plate and the closed rib plate, respectively) and the weld root are the potential fatigue-crack-initiating points affected by the weld size, plate thickness and weld penetration [19]. Moreover, the maximum principal stress distributions in the welding direction (welding direction is the red arrow route of the local B-B structure in Figure 5b) are shown in Figure 6, and the simulated stresses are from the FE model of the sub-model (Figure 4). The simulated results also indicate that the stress at the weld toe in the closed rib plate is significantly higher than those at weld toe in the diaphragm plate and the weld root. Therefore, the weld toe in the closed rib plate is considered as the interest point, and it is a potential fatigue-crack-initiating point during service condition of the bridge. In addition, the symmetrical principal stress curves in the weld toe in the rib plate may be caused by the boundary conditions applied to the sub-model. Moreover, the node position of weld toe in the rib plate is longer than the weld root and the weld toe in the diaphragm as shown in Figure 5b. Thus, the peak stress region of the weld toe in the rib plate does not line up with the peak stress regions for the weld root and the weld toe in the diaphragm plate.

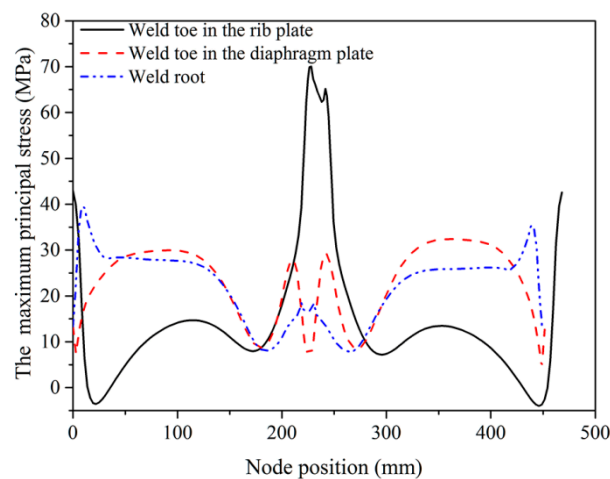


Figure 6. Stress–ode position curves of the rounded welding region in the sub-model (Node position is along the welding direction).

2.2. Fatigue Specimen

Based on the simulated stress distribution around the rounded welding region, we design a fatigue specimen of the structure detail with a rounded welding region (Figure 7). The material of fatigue specimen is Q345qD; it is a common steel material served as the bridge deck in China. In addition, the mechanical properties of the specimen material are shown in Table 1. Manual welding is employed to perform the welding, and the welding process parameters are listed in Table 2. Moreover, weld toes in the rib plate, the diaphragm plate, and the weld root are similar with weld details of the sub-model in Figure 5. In our simulation, the applied load is set as 50 kN. As shown in Figure 8, the maximum stress at the weld toe in the closed rib plate is higher than that at the weld root and the weld toe in the diaphragm plate. Because the weld length of our designed fatigue specimen is about half the length in sub-model (see node positions in Figures 6 and 8), the stress curves of the specimen welds are similar to the stress curves obtained from the sub-model (Figure 6). The similarity of the two stress distribution curves indicates the specimen can be used for the fatigue strength test of this weld detail.

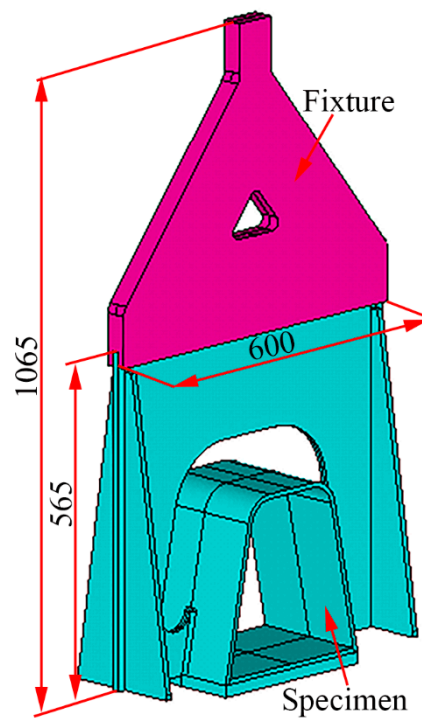


Figure 7. Specimen and fixture (in mm).

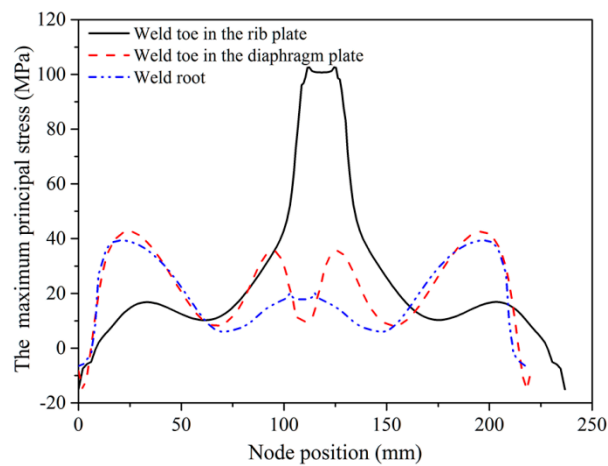


Figure 8. Stress–node position curves of the rounded welding region in the specimen.

Table 1. Mechanical properties of Q345qD.

Q345qD	Yield Strength (MPa)	Tensile Strength (MPa)	Elongation (%)	V notch Impact Energy (−20 °C, J)
	345	510	21	34

Table 2. Welding procedure.

Welding Processes	Manual Welding
Electrode diameter (mm)	Φ 4.0
Welding current (A)	160
Arc voltage (V)	24
Travel speed (cm/min)	30~40

2.3. Fatigue Tests and Results

In the rounded welding region of the fatigue specimen, strain rosettes are placed at a distance of approximately $1.5 t$ (t is the thickness of the closed rib) far away from the weld toe (Figure 9). In Figure 9a, the strain gauges 7 and 8 are used to determine the offset load caused by fabrication process. In Figure 9b, the strain rosettes 1–3 and 4–6 are distributed symmetrically, they can test the stress distribution of the weld toe in the rib plate. In addition, Figure 9c shows the photo of the fatigue specimen and the testing field. The fatigue tests are conducted by a hydraulic servo fatigue testing machine (SD-500, Changchun Research Institute for Mechanical Science CO. LTD, Changchun, China). During the testing, the load mode is the constant amplitude with a sine waveform at a frequency of 2 Hz, and the averaging stress ratio is about 0.06. Moreover, cameras with 40 magnifications are used to monitor and measure the crack initiation and propagation. In the fatigue test, fatigue cracks of the specimens firstly initiate from the rounded welding region between the diaphragm and closed rib, and the fatigue test results are summarized in Table 3. In addition, the stress range is measured by the strain rosettes 2 and 5 [20].

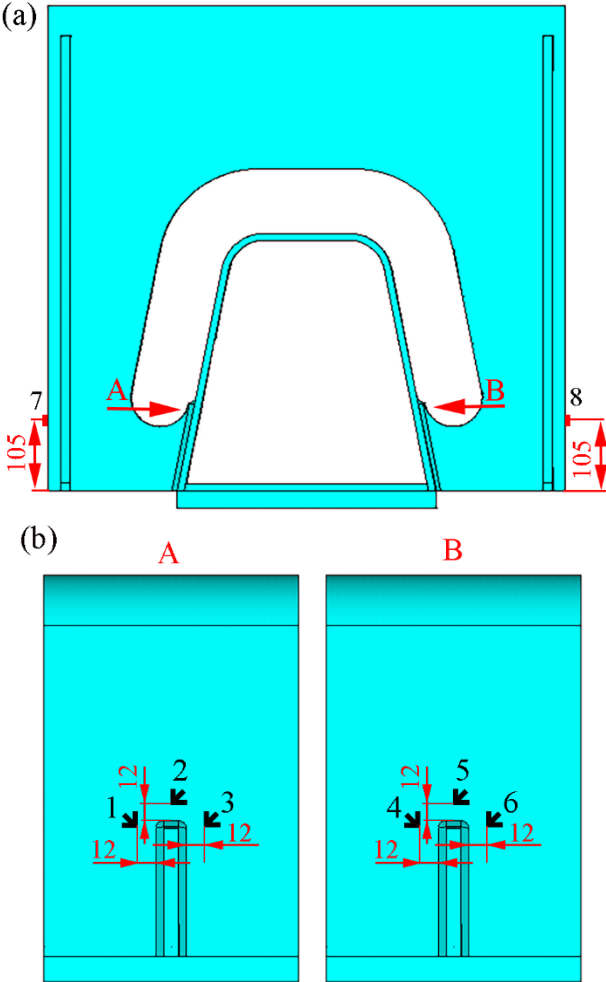


Figure 9. Cont.

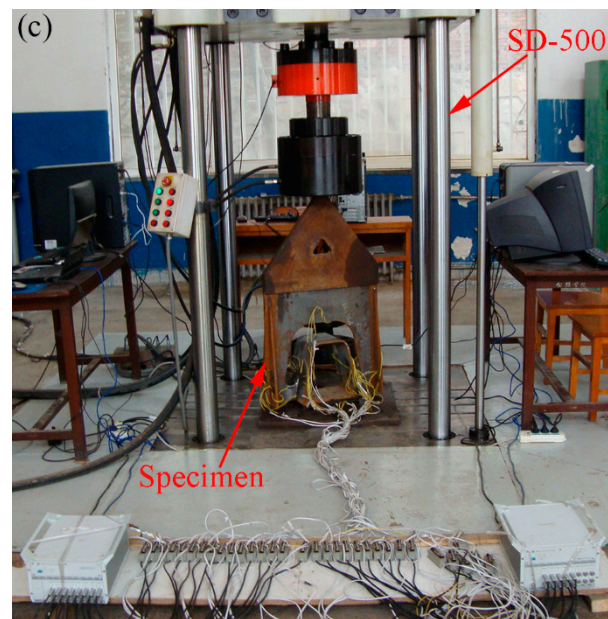


Figure 9. Schematic of the strain rosette location: (a) Strain gauges on the diaphragm, (b) Strain rosettes on the closed rib in A and B directions, respectively (in mm), (c) Photo of and the testing field and fatigue specimen.

Based on the fatigue results in Table 3, $\Delta\sigma$ -N equation is fitted by the least square method and the fatigue life curve with 50% confidence bound is given as following:

$$\lg N = 12.33 - 3.4 (\lg \Delta\sigma) \quad (1)$$

where fatigue cycles N are 2 million, the stress range $\Delta\sigma$ is about 59.32 MPa.

The fatigue life equation with 97.7% confidence bound is obtained by subtracting $2s$ (s is the standard deviation of $\lg N$, its value is 0.38) from the mean line of Equation (1):

$$\lg N = 11.57 - 3.4 (\lg \Delta\sigma) \quad (2)$$

where fatigue cycles N are 2 million, the stress range $\Delta\sigma$ is about 35.46 MPa. The $\Delta\sigma$ -N curves under two confidence bounds are plotted in Figure 10. Moreover, almost all cracks initiate from the rounded welding region between the diaphragm and the closed rib. We do not find a similar structure detail in the design codes for steel structures [21–24]. Therefore, Equation (2) could provide a reference for the fatigue design of this detailed structure.

Table 3. Fatigue test results.

Specimen ID	Minimum Stress (MPa)	Maximum Stress (MPa)	Stress Range $\Delta\sigma$ (MPa)	Number of Cycles N at Failure (Crack Reaches 30 mm)
SY-3-1-1	5.83	71.71	65.88	1409107
SY-3-1-2	5.83	104.65	98.82	1059280
SY-3-1-3	5.83	88.18	82.35	736535
SY-3-1-4	5.83	104.65	98.82	435607
SY-3-1-5	5.83	115.63	109.80	409925
SY-3-1-6	5.83	104.65	98.82	331072
SY-3-1-7	5.83	104.65	98.82	205567
SY-3-1-8	5.83	104.65	98.82	241068
SY-3-1-9	5.83	154.06	148.23	82632

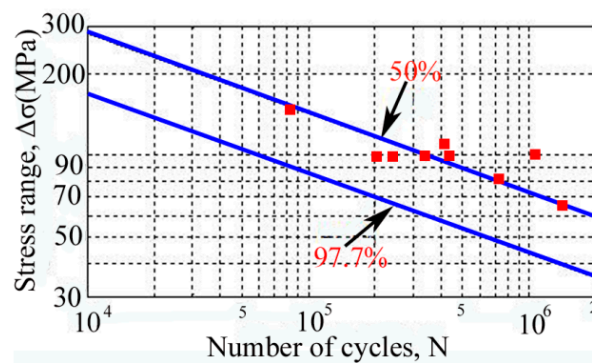


Figure 10. $\Delta\sigma$ -N curves of fatigue specimens.

3. Discussion

3.1. Fatigue Crack

The fatigue crack of the tested specimens initiates from the rounded welding region (Figure 11a), then the crack propagates along the weld toe (see red arrows in Figure 11b–d). Based on these fatigue tests observations, the weld toe in the closed rib plate is most susceptible to failure, therefore, the initiated position of the crack and the crack propagation path can indirectly demonstrate the validity of these fatigue specimens.

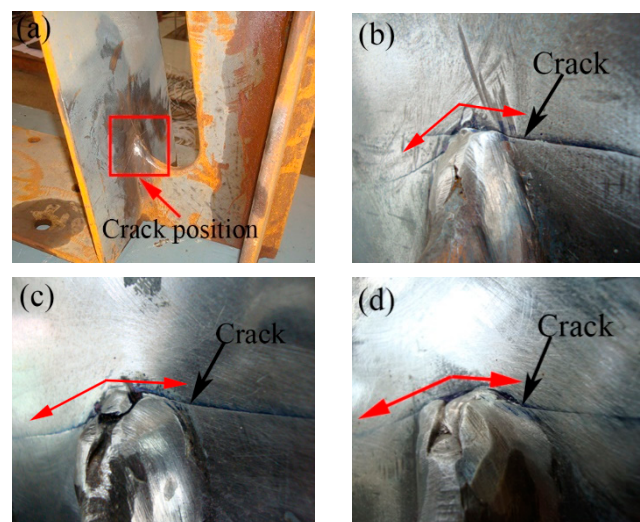


Figure 11. Cracks in the fatigue specimen: (a) Crack position in the specimen and Cracks of specimens (b) SY-3-1-2, (c) SY-3-1-5, (d) SY-3-1-6, respectively.

3.2. Hardness Measurements around the Crack

In order to analyze the mechanism of crack initiation, the hardness distribution of the welding region around the fatigue crack is measured by using a Vickers hardness tester [25–27] (Figure 12). The route of indentations successively crosses the parent metal (closed rib plate), heat-affected zone, weld toe (around the fatigue-crack-initiating point) and weld of specimen (from left to right in Figure 12b), and the distance between indentations is about 0.5 mm. Before the test, the surface of the specimen is well polished. In addition, the hardness distribution along the route reveals that the hardness fluctuates at the weld region (Figure 12b). However, the hardness value near the fatigue-crack-initiating point is about 200 HV, the value is slightly higher than the parent material's hardness (~180 HV). This phenomenon indicates the welding process has no significant effects on material hardness at the weld toe in the closed rib plate. But the maximum stress of the rounded

welding region still locates at the weld toe, then we get the conclusion that the stress concentration in the rounded welding region is the main mechanism of the fatigue crack initiation.

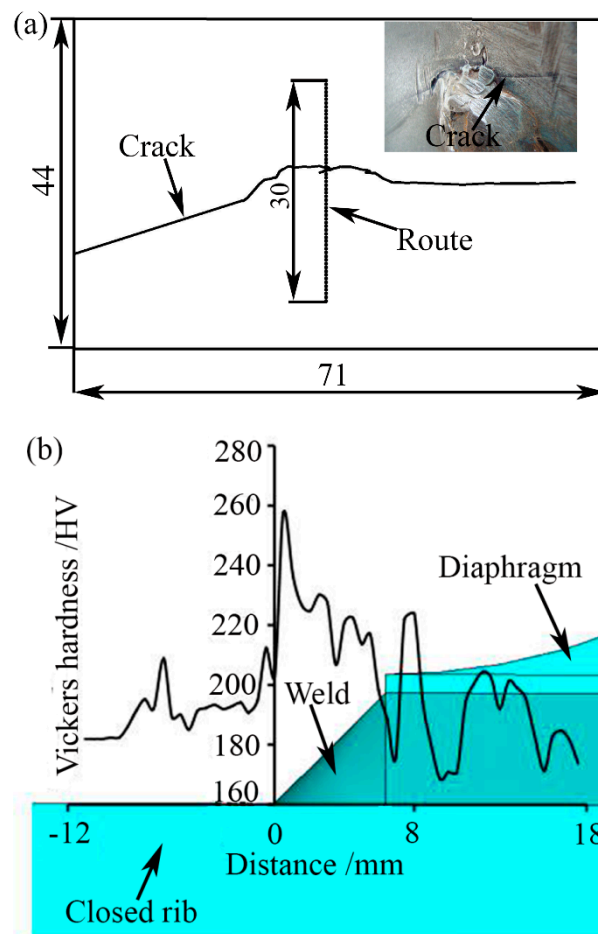


Figure 12. Vickers hardness test: (a) Sliced specimen (in mm) and (b) hardness distribution along the route.

3.3. Improvement of the Local Structure: Scheme 1

The previous analysis clearly states that the stress concentration is the major mechanism of fatigue crack initiation. Furthermore, we infer the stress concentration results from the size mutations between the diaphragm and the closed rib (see the arc in the diaphragm in Figure 1). Aiming to reduce the stress concentration, a reinforcing plate is incorporated onto the closed rib by welding. The details of the plate and the welding position are marked out in Figure 13a. With the purpose of reducing the peak value of the maximum principal stress in the rounded welding region, a parametric model in ANSYS software is developed to optimize the design parameters ($h1$, $h2$ and t , where t is the thickness of the reinforcing plate). Finally, the optimized results of the $h1$, $h2$ and t are 5 mm, 84 mm and 4 mm, respectively, and the maximum stress at the weld toe in the closed rib plate is 45.135 MPa in scheme 1 (Figure 13b). This value represents a decrease of 35.54% compared with the original peak stress. However, the stress at the weld toe in the diaphragm plate of the optimized reinforcing plate increases from 32.397 to 56.49 MPa (Figure 13b). The peak stress of the weld root is 39.65 MPa, and this value is very close to its original value. In summary, the stress concentration in the rounded welding region is reduced by welding the reinforcing plate. However, the stress at the weld toe in the diaphragm plate becomes larger than the stress at the weld toe in the rib plate. This means the expected failure location will change.

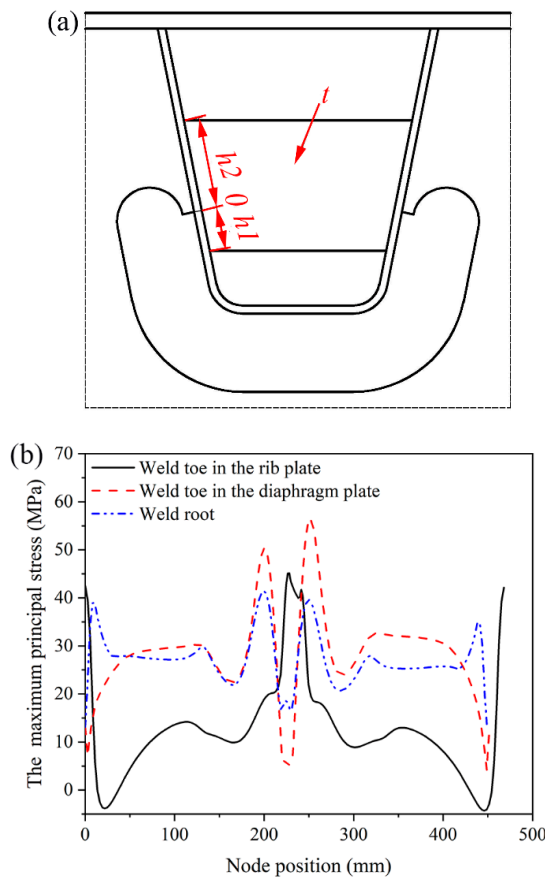


Figure 13. (a) Reinforcing plates in improvement scheme 1 and (b) stress–node position curves of the rounded welding region.

3.4. Improvement of the Local Structure: Scheme 2

In scheme 2, two reinforcing plates are installed on both sides of the closed rib by welding. The details of the reinforcing plates and the welding positions are identified in Figure 14a. Make sure the complete contact between the reinforcing plate and the closed rib, fusion-through welding is required. In this scheme, the plate thickness t_1 is larger than $(a_1 + a_2)/2$. Variables a_1 , a_2 , t_1 , and b are considered as design variables, while the state variable is the peak value of the maximum principal stress in the rounded welding region.

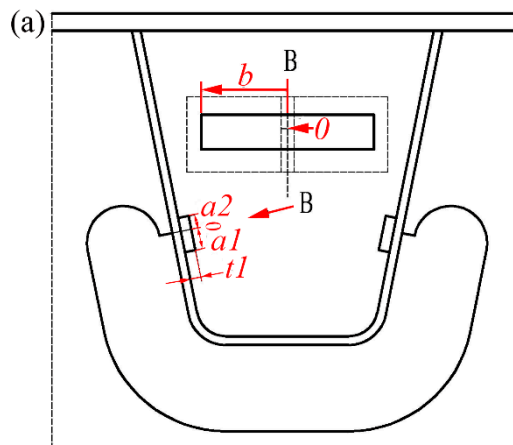


Figure 14. Cont.

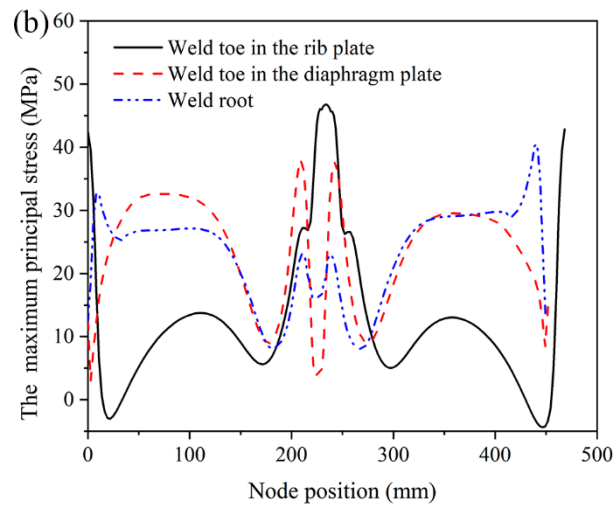


Figure 14. (a) Reinforcing plates in improvement scheme 2 and (b) stress—node position curves of the rounded welding region.

Furthermore, the optimized results of the $a1$, $a2$, $t1$, and b are 13 mm, 14 mm, 14 mm, and 135 mm, respectively, and the maximum stress at the weld toe in the closed rib plate is 46.711 MPa in scheme 2 (Figure 14b). This value represents a decrease of 33.29% compared with the original maximum stress. The maximum stress at weld toe in the diaphragm plate is 37.99 MPa and increases by 5.593 MPa (an increase of 17.26%) as compared with the original value. The peak stress at weld root is 40.51 MPa and increases by 1.151 MPa (an increase of 2.9%). In this scheme, the stress concentration in welded region is reduced, while the peak stresses at the weld toe in the diaphragm plate and weld root also increase.

3.5. Improvement of the Local Structure: Scheme 3

In scheme 3, two reinforcing plates are welded on both sides of the closed rib, respectively. We can see the details of reinforcing plates and the welding positions in Figure 15a. An original point is chosen (marked as “0”) for optimizing the dimensions of the reinforcing plate. Fusion-through welding is also required, thus the plate thickness $t2$ should be larger than $b1$. The variables $a3$, $a4$, $t2$, and $b1$ are considered as design variables, and the state variable still is the peak value of the maximum principal stress in the rounded welding region.

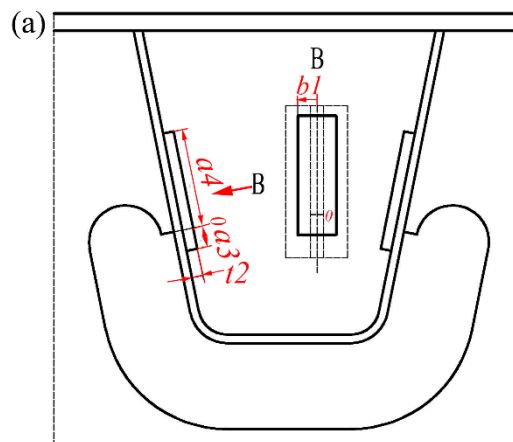


Figure 15. Cont.

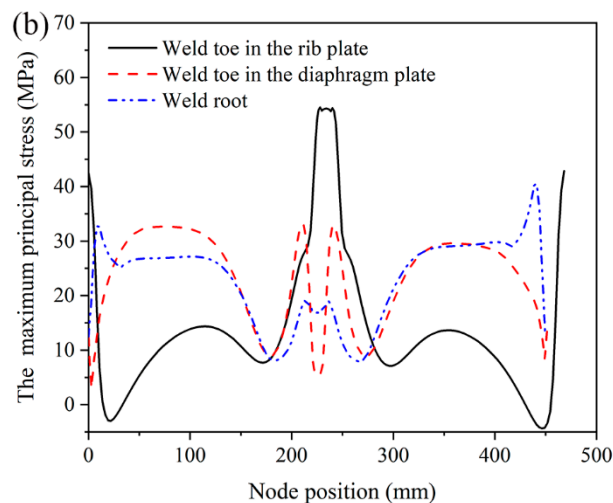


Figure 15. (a) Reinforcing plates in improvement scheme 3 and (b) stress—node position curves of the rounded welding region.

Finally, the optimized results of the a_3 , a_4 , t_2 , and b_1 are 12 mm, 15 mm, 11.5 mm, and 21 mm, respectively, and the peak stress at the weld toe in the rib plate is 52.8 MPa in scheme 3 (Figure 15b). This value means a decrease of 24.6% compared with the original peak stress. The peak stress at weld toe in the diaphragm plate is 32.673 MPa and increases 0.276 MPa (an increase of 0.85%) as compared with the original value. The peak stress at weld root increases from 39.359 to 40.532 MPa. In this scheme, the reinforcing plate reduces the stress concentration in welded region, but the peak stress at the weld toes in the diaphragm and the weld root does not significantly increase.

3.6. Comparisons of Three Improvement Schemes

Following the above descriptions, distribution curves of the maximum principal stress for the weld toe in the closed rib plate, the weld toe for the diaphragm plate and the weld root of three improvement schemes are plotted in Figure 16a–c, respectively. Moreover, the maximum principal stresses of the rounded welding regions with and without reinforcing plate are listed in Table 4. For the rounded welding region, three improvement schemes can effectively reduce the stress concentration at the weld toe in the closed rib plate. However, the scheme 2 is better than the schemes 1 and 3. Because both schemes 1 and 2 reduce the peak stress more than scheme 3, but scheme 1 increases the stress at the weld toe in the diaphragm plate to be more than the stress at the weld toe in the closed rib plate. Thus, we consider scheme 2 is the best and effectively improve the fatigue resistance of the rounded welding region of the diaphragm–rib structure.

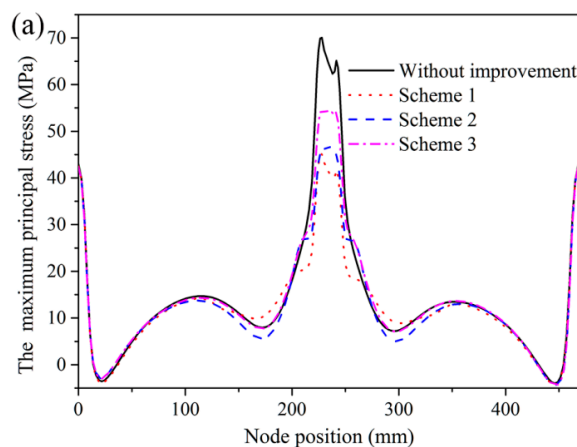


Figure 16. Cont.

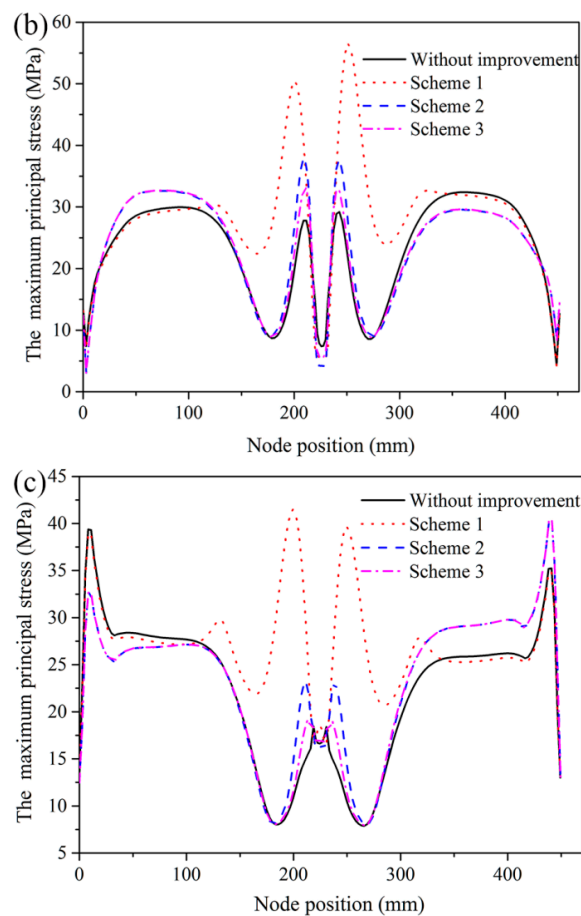


Figure 16. Stress–node position curves in the rounded welding region before and after improvement: Stress curves of (a) weld toe in the closed rib plate, (b) weld toe in the diaphragm plate and (c) weld root.

Table 4. Peak value of the maximum principal stress in the rounded welding region before and after improvement.

Locations	Schemes			
	Without Improvement	Scheme 1	Scheme 2	Scheme 3
Weld toe in the closed rib plate (MPa)	70.023	45.135	46.711	52.8
Weld toe in the diaphragm plate (MPa)	32.397	56.49	37.99	32.673
Weld root (MPa)	39.359	39.65	40.51	40.532

4. Conclusions

In this study, the fatigue performance of the rounded welding region between diaphragm plate and closed rib of an orthotropic steel bridge deck is investigated using experimental methods and FEM. The main conclusions are summarized as follows

- (1) The fatigue crack of the rounded welding region of the orthotropic steel bridge deck initiates from the weld toe in the closed rib plate.
- (2) The fatigue strength equation for the tested specimens is $\lg N = 11.57 - 3.4(\lg \Delta \sigma)$ with 97.7% confidence bound. When the fatigue cycles N is 2 million, the stress range $\Delta \sigma$ is 35.46 MPa. This equation can provide a reference for the fatigue design of this detailed structure.
- (3) The stress concentration of the rounded welding region is the main mechanism of fatigue crack initiation. Two optimized reinforcing plates welded in the closed rib effectively reduce the stress

concentration of the rounded welding region, and the fatigue strength of this welded structure can be enhanced.

Author Contributions: Writing—original draft preparation, D.L.; writing—review and editing, C.Z.; supervision, P.L. All authors have read and agreed to the published version of the manuscript.

Funding: This research was funded by the Project of Jiangxi Provincial Communication Department, grant number 2010C00003. This research was also funded by the National Natural Science Foundation of China, grant number 11902046 and the Fundamental Research Funds for the Central Universities, CHD, grant number 300102259302.

Conflicts of Interest: The authors declare no conflict of interest.

References

1. Freitas, S.T.D.; Kolstein, H.; Bijlaard, F. Composite bonded systems for renovations of orthotropic steel bridge decks. *Compos. Struct.* **2010**, *92*, 853–862. [[CrossRef](#)]
2. Kainuma, S.; Yang, M.; Jeong, Y.S.; Inokuchi, S.; Kawabata, A.; Uchida, D. Experiment on fatigue behavior of rib-to-deck weld root in orthotropic steel decks. *J. Constr. Steel Res.* **2016**, *119*, 113–122. [[CrossRef](#)]
3. Huang, Y.; Zhang, Q.; Bao, Y.; Bu, Y. Fatigue assessment of longitudinal rib-to-crossbeam welded joints in orthotropic steel bridge decks. *J. Constr. Steel Res.* **2019**, *159*, 53–66. [[CrossRef](#)]
4. Choi, J.H.; Kim, D.H. Stress characteristics and fatigue crack behaviour of the longitudinal rib-to-cross beam joints in an orthotropic steel deck. *Adv. Struct. Eng.* **2008**, *11*, 189–198. [[CrossRef](#)]
5. Zhang, Q.H.; Cui, C.; Bu, Y.Z.; Liu, Y.M.; Ye, H.W. Fatigue tests and fatigue assessment approaches for rib-to-diaphragm in steel orthotropic decks. *J. Constr. Steel Res.* **2015**, *114*, 110–118. [[CrossRef](#)]
6. Cui, C.; Zhang, Q.; Luo, Y.; Hao, H.; Li, J. Fatigue reliability evaluation of deck-to-rib welded joints in OSD considering stochastic traffic load and welding residual stress. *Int. J. Fatigue* **2018**, *111*, 151–160. [[CrossRef](#)]
7. Zhang, Q.; Bu, Y.; Li, Q. Review on fatigue problems of orthotropic steel bridge deck. *J. China J. Highw.* **2017**, *30*, 14–30.
8. Deng, Y.; Liu, Y.; Feng, D.; Li, A. Investigation of fatigue performance of welded details in long-span steel bridges using long-term monitoring strain data. *Struct. Control. Health Monit.* **2015**, *22*, 1343–1358. [[CrossRef](#)]
9. Alemdar, F. Experimental Study of Fatigue Crack Behavior of Rib-To-Rib Butt Welded Connections in Orthotropic Steel Decks. *Lat. Am. J. Solids Struct.* **2018**, *15*, e128.
10. Zhuang, M.; Miao, C.; Chen, R. Analysis for Stress Characteristics and Structural Parameters Optimization in Orthotropic Steel Box Girders based on Fatigue Performance. *KSCE J. Civ. Eng.* **2019**, *23*, 2598–2607. [[CrossRef](#)]
11. Tsakopoulos, P.A.; Fisher, J.W. Full-scale fatigue tests of steel orthotropic decks for the Williamsburg Bridge. *J. Bridge Eng.* **2003**, *8*, 323–333. [[CrossRef](#)]
12. Connor, R.J.; Fisher, J.W. Consistent approach to calculating stresses for fatigue design of welded rib-to-web connections in steel orthotropic bridge decks. *J. Bridge Eng.* **2006**, *11*, 517–525. [[CrossRef](#)]
13. Xiao, Z.; Yamada, K.; Ya, S.; Zhao, X. Stress analyses and fatigue evaluation of rib-to-deck joints in steel orthotropic decks. *Int. J. Fatigue* **2008**, *30*, 1387–1397. [[CrossRef](#)]
14. Ya, S.; Yamada, K.; Ishikawa, T. Fatigue evaluation of rib-to-deck welded joints of orthotropic steel bridge deck. *J. Bridge Eng.* **2010**, *16*, 492–499. [[CrossRef](#)]
15. Sim, H.; Uang, C.; Sikorsky, C. Effects of fabrication procedures on fatigue resistance of welded joints in steel orthotropic decks. *J. Bridge Eng.* **2009**, *14*, 366–373. [[CrossRef](#)]
16. Miki, C. Fatigue damage in orthotropic steel bridge decks and retrofit works. *Int. J. Steel Struct.* **2006**, *6*, 255–267.
17. Zhang, Q.; Liu, Y.; Bao, Y.; Jia, D.; Bu, Y.; Li, Q. Fatigue performance of orthotropic steel-concrete composite deck with large-size longitudinal U-shaped ribs. *Eng. Struct.* **2017**, *150*, 864–874. [[CrossRef](#)]
18. JTGD60-2004. *General Code for Design of Highway Bridges and Culverts*; China Communications Press: Beijing, China, 2004.
19. Zhang, C.; Lu, P.; Hu, X.; Song, X. Effect of buffer layer and notch location on fatigue behavior in welded high-strength low-alloy. *J. Mater. Process. Technol.* **2012**, *212*, 2091–2101. [[CrossRef](#)]
20. Hobbacher, A. *Recommendations for Fatigue Design of Welded Joints and Components*; Springer: Berlin/Heidelberg, Germany, 2009.

21. GB50017-2003. *Code for Design of Steel Structures*; China Architecture & Building Press: Beijing, China, 2003.
22. TB10002-2. *China Railway Major Bridge Reconnaissance Design of Railway Bridge*; China Railway Publishing House: Beijing, China, 2005.
23. Nussbaumer, A.; Borges, L.; Davaine, L. *Fatigue Design of Steel and Composite Structures: Eurocode 3: Design of Steel Structures, Part 1–9 Fatigue; Eurocode 4: Design of Composite Steel and Concrete Structures*; John Wiley & Sons: Hoboken, NJ, USA, 2012.
24. *AASHTO LRFD Bridge Design Specifications*, 6th ed.; Parts I and II; ASCE: Atlanta, GA, USA, 2012.
25. Ghorbal, G.B.; Tricoteaux, A.; Thuault, A.; Louis, G.; Chicot, D. Comparison of conventional Knoop and Vickers hardness of ceramic materials. *J. Eur. Ceram. Soc.* **2017**, *37*, 2531–2535. [[CrossRef](#)]
26. Moreira, F.D.L.; Kleinberg, M.N.; Arruda, H.F.; Freitas, F.N.C.; Parente, M.M.V.; De Albuquerque, V.H.C.; Rebouças, P.P. A novel Vickers hardness measurement technique based on Adaptive Balloon Active Contour Method. *Expert Syst. Appl.* **2016**, *45*, 294–306. [[CrossRef](#)]
27. Guo, B.; Zhang, L.; Cao, L.; Zhang, T.; Jiang, F.; Yan, L. The correction of temperature-dependent Vickers hardness of cemented carbide base on the developed high-temperature hardness tester. *J. Mater. Process. Technol.* **2018**, *255*, 426–433. [[CrossRef](#)]



© 2020 by the authors. Licensee MDPI, Basel, Switzerland. This article is an open access article distributed under the terms and conditions of the Creative Commons Attribution (CC BY) license (<http://creativecommons.org/licenses/by/4.0/>).